Chem

CellPress
OPEN ACCESS

Article

Robotic synthesis of peptides containing metal-oxide-based amino acids

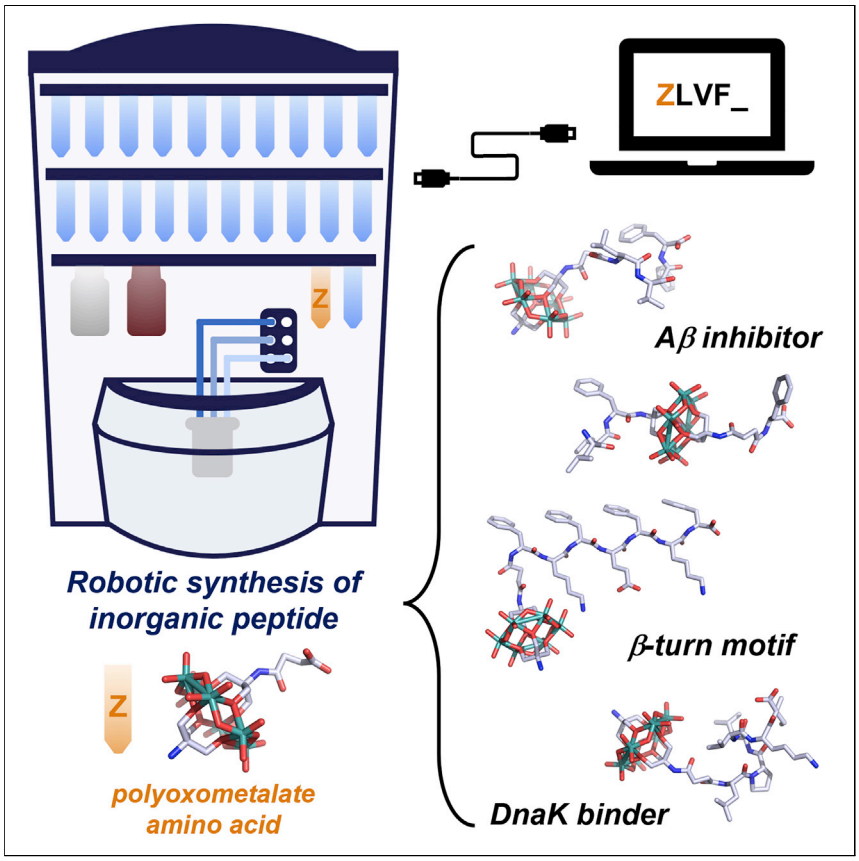

The incorporation of non-coded amino acids into peptide sequences could be important for the fields of protein engineering and hybrid biomaterials. Herein, we report a robotic platform that allows the programmable insertion of a non-coded polyoxometalate amino acid into various peptide sequences, thus fabricating a wide range of inorganic peptides with enhanced biofunctionalities. The platform is automatic and efficient and uses commercially available equipment.

Shan She, Nicola L. Bell, Dazhong Zheng, ..., De-Liang Long, Jesko Koehnke, Leroy Cronin

lee.cronin@glasgow.ac.uk

Highlights

Develops a scalable POM-based amino acid accessible for solid-phase peptide synthesis

Achieves robotic synthesis of diverse POM peptides in a commercial synthesizer

Enhances biofunctionality of anionic POM peptides through precise sequence control

Exploits POM-based Aβ inhibitor, β turn assembly, and strong binder with DnaK protein

She et al., Chem 8, 1–15
October 13, 2022
Published by Elsevier Inc.
https://doi.org/10.1016/j.chempr.2022.07.007

Please cite this article in press as: She et al., Robotic synthesis of peptides containing metal-oxide-based amino acids, Chem (2022), https://doi.org/10.1016/j.chempr.2022.07.007

Chem

Article

Robotic synthesis of peptides containing metal-oxide-based amino acids

Shan She,[1] Nicola L. Bell,[1] Dazhong Zheng,[1] Jennifer S. Mathieson,[1] Maria D. Castro,[1] De-Liang Long,[1] Jesko Koehnke,[1] and Leroy Cronin[1,2,*]

SUMMARY

Peptides display a range of important properties, controlled by the intrinsic nature of organic side chains, regarding redox activity, charge density, and structure. Here, we demonstrate a new synthetic approach to insert non-coded amino acids that contain metal oxide groups into a desired peptide sequence with a commercial peptide synthesizer. This approach allowed us to design and isolate a range of highly anionic peptides with various sequences, including the amyloid Aβ_{17-20}, the amphiphilic KFE8, and a bacterial chaperone DnaK substrate. By taking advantage of both the inorganic polyoxometalate-based motif and the peptide sequence, the resultant POM peptides enable significant inhibition of amyloid aggregation, switch a β sheet into a β turn, and enhance binding with the molecular chaperone DnaK. Therefore, we show it is possible to program the robotic synthesis of peptides with functional inorganic amino acids as a generic approach for the design and exploration of next-generation artificial biological-inorganic structures.

INTRODUCTION

The robotic synthesis of functional molecules and assemblies is becoming increasingly important to aid the search of chemical and biochemical space in a reproducible and scalable manner.[1–7] An important strategy in the design and construction of robotic synthesis paradigms[1,2,8] is to exploit existing commercially available robotic synthesis equipment.[9] For example, commercial peptide synthesizers are widely used for solid-phase synthesis because of the possibility to circumvent the often tedious and time-consuming isolation of intermediates and products.[3–5,7] Furthermore, this programmable approach has been employed to configure complex peptide synthesis reactions through coupling-deprotection reactions of natural amino acid derivatives.[3] A variety of peptides have been fabricated in a combinatorial fashion to explore biochemical mechanisms,[10,11] develop new functional materials,[12,13] and create artificial enzymes.[14,15] To further improve bioactivity, bioavailability, and structural diversity, many unnatural inorganic residues—including metal clusters,[16–18] polyhedral oligomeric silsesquioxane (POSS),[19] and oligonuclear transition metal coordination complexes[18,20,21]—have been incorporated as non-canonical amino acids into peptide sequences through manual synthesis. This is important since such compounds can serve as spectroscopic or photo-affinity probes for bioassays,[18–20] cancer diagnoses,[16,17] and cancer-targeted therapy.[21,22] However, there is a lack of configurability regarding charge density, redox activity, and the introduction of radical new structures and coordination systems.[23]

Anionic peptides have attracted a lot of attention since they are important components in proteins to interact with inorganic surfaces,[24,25] acting as antimicrobial

THE BIGGER PICTURE

Protein engineering has undergone a revolution due to our understanding of how peptide sequences can be modeled, folded, and utilized as functional units. A route to insert inorganic motifs using robotic synthesis would be transformative, since such moieties could have a profound effect on the structure, charge density, redox properties, as well as the conformational flexibility of the resulting peptide or protein. Here, we show it is possible to program the incorporation of inorganic POM amino acid using a commercial peptide synthesizer to readily prepare a series of inorganic peptides automatically and efficiently. Furthermore, the optimized combination between inorganic POM motif and organic peptide sequence also enables the exploration for optimized POM peptides with new functions, including inhibition of amyloid aggregation, conformational switching of β sheet to β turn, and enhanced binding with the DnaK protein.

Please cite this article in press as: She et al., Robotic synthesis of peptides containing metal-oxide-based amino acids, Chem (2022), https://doi.org/10.1016/j.chempr.2022.07.007

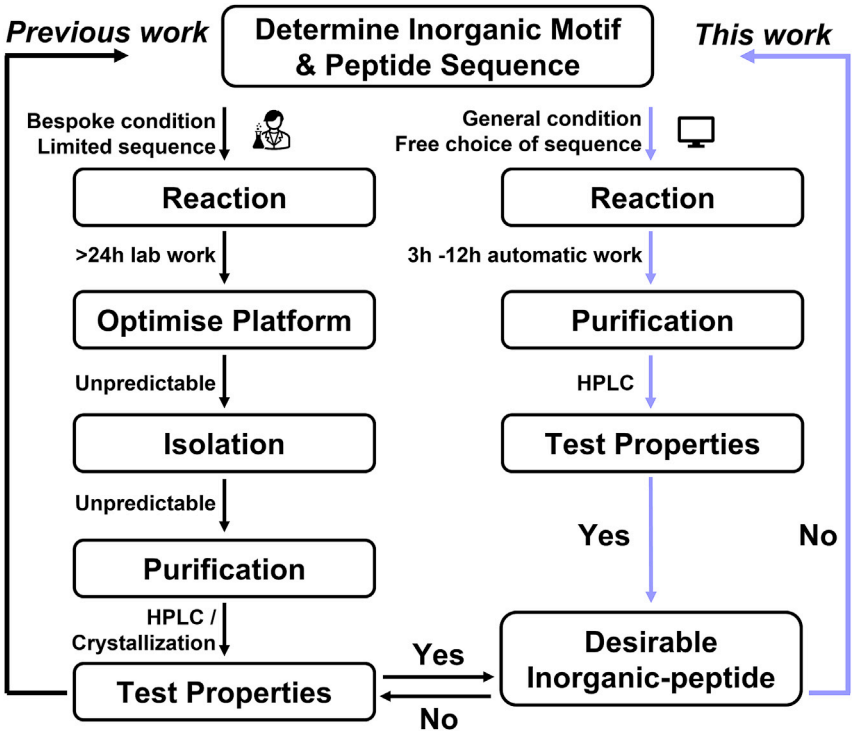

Figure 1. Synthesis cycle for peptides containing inorganic motif

Compared with the previous manual method, this work demonstrates an automatic, high-efficiency, easy access cycle to explore unknown inorganic peptides.

agents against bacteria and fungi,[26] and at the same time they could play an important role in the inhibition of diseases such as Alzheimer disease and Parkinson disease.[27] However, due to the complex synthetic processes for inorganic amino acids, which is limited to specific amino acids,[28,29] no general routes exist to incorporate anionic inorganic amino acid residues into a peptide chain automatically under robotic control. To achieve this goal, we chose polyoxometalates (POMs), a large group of clusters built from multiple transition metal ions linked by shared oxo or hydroxo anions;[30] their molecular nature means they introduce higher charge densities,[31] redox activity,[32,33] and additional coordination/catalytic sites into the peptide chain,[34] leading to exciting new opportunities for protein biochemistry and inorganic medicinal chemistry.[35–38] Incorporation of redox-active POMs into sequences may further impart POM peptides with tuneable redox responsiveness, which is useful in redox bio-catalysis, redox-mediated self-assembly, and hybrid flow battery. To date there are two major methodologies to introduce POMs into peptide chains: non-covalent assembly[34,39,40] or covalent conjugation.[28,29,36–38] However, the bespoke conditions required, unpredictable reactions, and the potential for many by-products greatly limit the exploration of biochemical activity of hybrid inorganic peptides (see Figure 1).

Marrying automation technology to inorganic chemistry, we envisioned that there could be a great opportunity to incorporate inorganic programmable amino acids into a commercial peptide synthesizer, offering a platform for the automated synthesis of inorganic peptides exploiting solid-phase peptide synthesis (SPPS) systems (Figure 1). Previously reported systems mainly utilized the manual synthesis of POM peptides in the solution phase.[28,29,39,41] However, the multi-step

[1]School of Chemistry, University of Glasgow, Glasgow G12 8QQ, UK

[2]Lead contact

*Correspondence: lee.cronin@glasgow.ac.uk

https://doi.org/10.1016/j.chempr.2022.07.007

Please cite this article in press as: She et al., Robotic synthesis of peptides containing metal-oxide-based amino acids, Chem (2022), https://doi.org/10.1016/j.chempr.2022.07.007

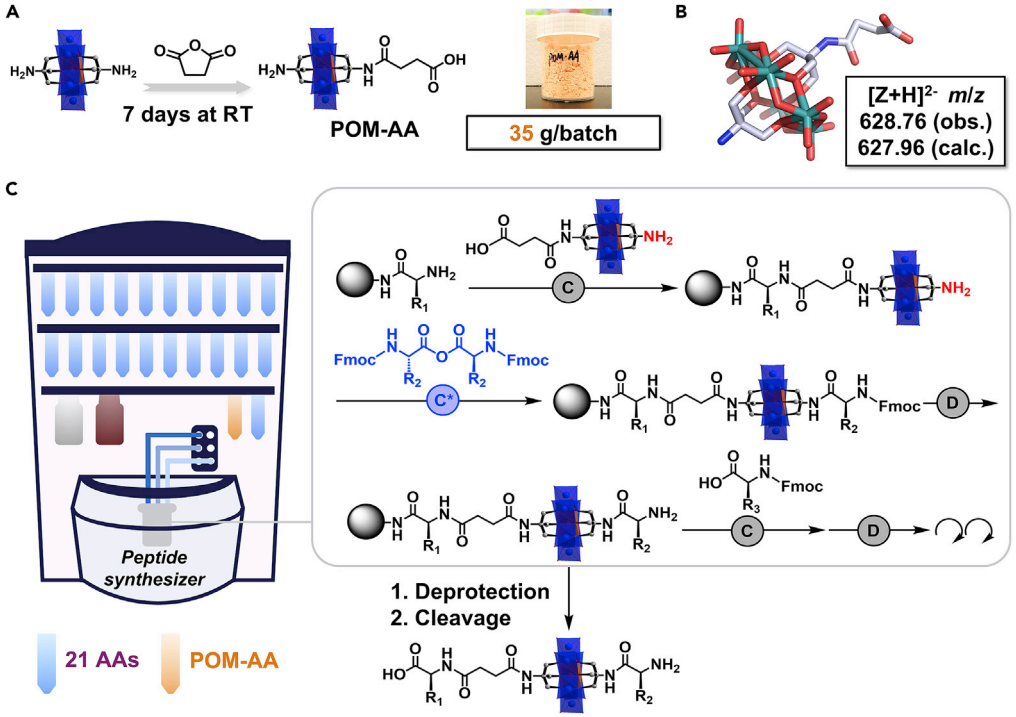

Figure 2. Schematic representation of POM-AA and POM-peptide synthesis procedure

(A) Design and fabrication of POM-AA and its six advantageous features (mild synthesis condition, high yield 92%, readily scalable, Fmoc protection-free, column separation-free, and O_2 and H_2O stable).

(B) Single-crystal structure and ESI-MS number of POM-AA. Hydrogen atoms and $3TBA^+$ counter cations are omitted for clarity.

(C) Automated synthesis of POM peptide on a typical peptide synthesizer. The syntheses are shown with the respective conditions and the fundamental unit operations required in each step.

Abbreviations are as follows: C, standard coupling (4 equiv amino acid, 4.4 equiv DIC, and 4.4 equiv HOBt, 75°C), D, standard deprotection (20% piperidine in DMF, room temperature [RT]); C*, anhydride coupling (4 equiv amino acid anhydride, 2.5 equiv DIPEA, 75°C).

preparation and time-consuming column separation with low overall yield (ca. 26%, 0.5 g) of POM precursors (Scheme S1) greatly limited any practical applications. Herein, we demonstrate the preparation of a functionalized POM through a one-step, column-free synthesis, which can serve as an "inorganic amino acid" flanked by an amine ($–NH_2$) and a carboxylic acid (–COOH) group at each terminal position (Figure 2A, POM-AA). This POM-AA, based on a Mn-Anderson POM moiety $\{Mn^{III}Mo^{VI}_6O_{24}\}$,[28] is easily synthesized, readily scalable (up to 92%, 35 g), inexpensive, and, importantly, tolerant to standard coupling and deprotection conditions. Through the incorporation of POM-AA into a commercial peptide synthesizer system (Figure 2C), a variety of POM peptides were readily prepared (vide infra). This proved that the new residue could be placed almost anywhere in the sequence using an automated system, and this enabled us to explore both natural and artificial peptide sequences with POM-AA.

RESULTS AND DISCUSSION

Synthesis and characterization of the POM-AA

A variety of POM nanoclusters, including Keggin, Dawson, Lindqvist, Weakley, and Anderson types, have been widely employed in the design and fabrication of organic-inorganic hybrid materials.[41] Among them, a Tris-bifunctionalized Anderson POM was chosen for this research, on account of its easy modification and scalable preparation.[41,42] More importantly, we found that the protection of the

Please cite this article in press as: She et al., Robotic synthesis of peptides containing metal-oxide-based amino acids, Chem (2022), https://doi.org/10.1016/j.chempr.2022.07.007

N terminus can be circumvented on this POM (Figure S25; Scheme S2). Based on it, we designed the POM-AA with an amine ($-NH_2$) without Fmoc protection, which saved a lot of effort both in POM-AA preparation and the following POM-peptide synthesis process. The preparation of POM-AA is straightforward and is easily accessed by reaction of the Tris-bifunctionalized Anderson POM with succinic anhydride (Figure 2A) under mild conditions (RT, 7 days), which gives the non-symmetric POM-AA (Z) in high yield (92%) through precipitation as an air-stable orange powder (Scheme S1). Notably, the synthesis is very scalable up to 35 g/batch, and this can provide ample material for an automatic synthesis conducted in a peptide synthesizer (~1.5 g/0.1 mmol coupling). The single-crystal structure of POM-AA (Figure 2B) demonstrated the asymmetric modification of the POM with an $-NH_2$ group as an Fmoc-free N terminus and a carboxylate moiety as C terminus. ESI-MS characterization of this POM-AA (Figures 2B, S1, and S2) yielded a *m/z* peak at 628.76 that shows a good match with that calculated for $\{[MnMo_6O_{24}(C_8H_{12}NO_3)(C_4H_8N)]H\}^{2-}$ at 627.96 (Table S2), corresponding to the anionic form of $[(POM\text{-}AA) + H]^{2-}$. Notably, the inorganic POM-AA is oxygen and water stable and thus can be stored at room temperature in air.

Automated synthesis of POM peptides

Automated synthesis of POM peptides was implemented through SPPS with Biotage Initiator + Alstra Automated Microwave Peptide Synthesizer in a single reaction vessel and executed by its built-in software, thus providing an easy user interface for a non-specialist. Through standard DIC/HOBt coupling (Figure 2C), the canonical amino acid ($-R_1$) and POM-AA are grafted onto the growing peptide chain on TentaGel S Trt resins in sequence. The unprotected N terminus of the POM-AA is unreactive toward DIC/HOBt coupling, therefore the introduction of the subsequent canonical amino acid ($-R_2$) is achieved through anhydride coupling (whereby the anhydride derivative of the amino acid residue is employed). We incorporated the next amino acids using the standard DIC/HOBt coupling. Finally, the cleavage of POM peptide from resin is carried out using 1,1,1,3,3,3-hexafluoro-2-propanol (HFIP)/DCM (20% v/v), as strong cleavage conditions such as TFA/TIS/H_2O can destabilise the Anderson clusters.[28] However, the HFIP/DCM cocktail is unable to remove classical protecting groups (e.g., Boc, *t*Bu) from side-chain residues. Instead, we chose Mmt (monomethoxytrityl) and Alloc/Oall-protected amino acids as alternatives, which can be mildly cleaved by AcOH/TFE/DCM and Pd(0)/AcOH/NMP/$CHCl_3$, respectively. POM-AA also proved to be stable in the above cleavage cocktails, and this was confirmed by ESI-MS (Figure S26). After complete deprotection and cleavage steps, the resultant POM peptides were purified by preparative liquid chromatography (CH_3CN/H_2O). Thus, we can automate the synthesis with a wide range of POM peptides within a commercial peptide synthesizer much easier and quicker with the whole process taking 3–12 h, compared with >24 h lab work previously.

POM peptides designed to inhibit Aβ aggregation

One of the great advantages of using POM-AA in an automated synthesizer is the ability to achieve precise positional control. The natural sequence ($A\beta_{17-20}$, LVFF) is the key aggregation core of β-amyloid (Aβ) fibers,[43] and this is thought to be a potential cause of Alzheimer disease. In this respect, it has been shown that highly negatively charged POMs (e.g., $[P_2CoW_{17}O_{61}]^{8-}$, $[P_2NiW_{17}O_{61}]^{8-}$, α-$[SiW_9O_{34}]^{10-}$) can inhibit Aβ aggregation because of electrostatic interactions between the POM anions and the cationic domain ($A\beta_{13-16}$, HHQK) alongside the aggregation core ($A\beta_{17-20}$, LVFF).[44–46] Importantly, POMs and their derivatives are capable of penetrating through the blood-brain barrier, addressing the major

Please cite this article in press as: She et al., Robotic synthesis of peptides containing metal-oxide-based amino acids, Chem (2022), https://doi.org/10.1016/j.chempr.2022.07.007

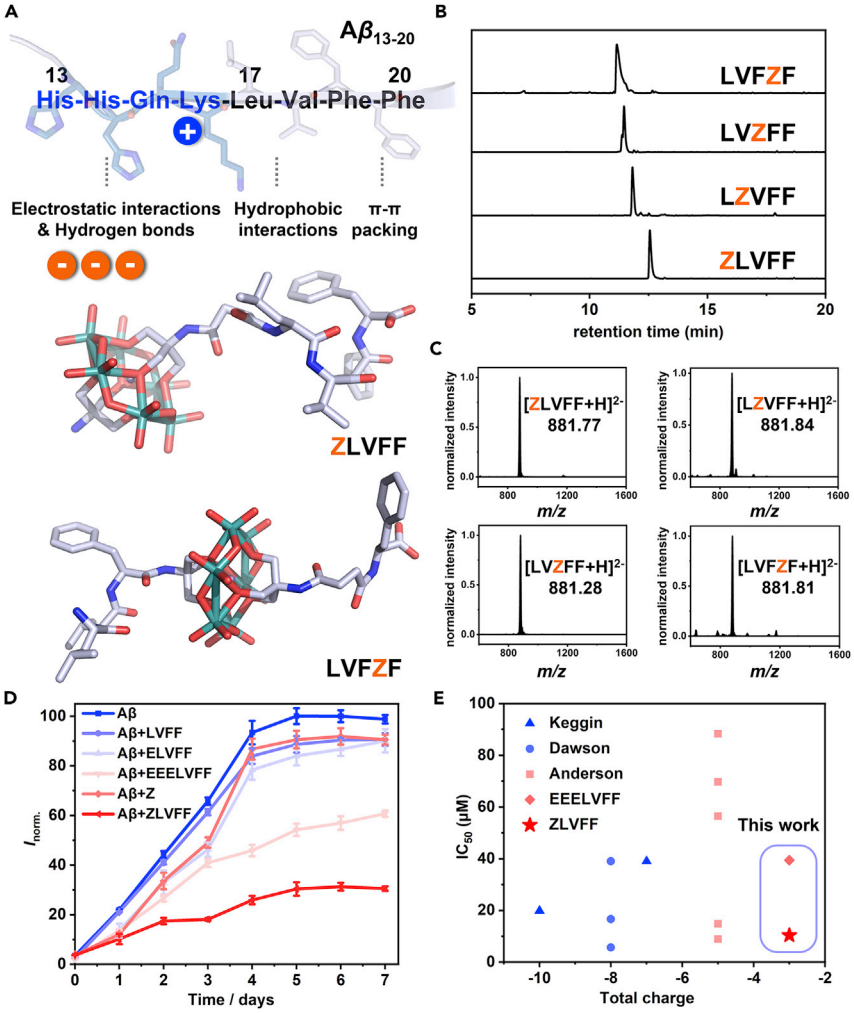

Figure 3. Rationally designed POM peptides and its inhibition toward Aβ_{1-40} aggregation

(A) Schematic representation of ZLVFF series with positional control of Z amino acid in the peptide sequence and its potential as hybrid inhibitors toward Aβ_{1-40} aggregation based on the multiple interactions.

(B) LC trace of ZLVFF, LZVFF, LVZFF, LVFZF obtained from analytic HPLC in the solvent system of CH_3CN/H_2O/FA.

(C) Corresponding ESI-MS spectra with observed *m/z* values of their anions, and calculated *m/z* value is 881.65, assigned to $\{[MnMo_6O_{24}(C_{41}H_{58}N_6O_7)]H\}^{2-}$.

(D) Aggregation kinetics of Aβ_{1-40} monitored by ThT fluorescence; concentrations of Aβ and ligands are 40 and 20 μM, respectively. The experiments were conducted three times.

(E) Comparison of IC_{50} values of ZLVFF toward previously reported inhibitors; we present the lowest IC_{50} value for each POM catalogs (1) Keggin, $Na_9H[SiW_9O_{34}]$, total charge −10, IC_{50} = 19.85;[44] (2) Dawson, POMs-Dawson-Ni, total charge −8, IC_{50} = 5.67;[45] (3) Anderson, POM-L-Phe, total charge −5, IC_{50} = 14.86;[46] (4) peptide, EEELVFF, total charge −3, IC_{50} = 39.40; and (5) Anderson-peptide, ZVFF, total charge −3, IC_{50} = 10.36.

problem in molecular therapy of neurodegenerative diseases, which further promotes their research in Alzheimer treatment.[45–47] To build on this, the POM-AA (labeled as Z) was introduced into 4 different positions of the natural peptide sequence of Aβ_{17-20}, H_2N-Leu-Val-Phe-Phe-OH (LVFF) so we could investigate its potential in creating hybrid inhibitors for Aβ_{1-40} aggregation (see Figure 3A).

Please cite this article in press as: She et al., Robotic synthesis of peptides containing metal-oxide-based amino acids, Chem (2022), https://doi.org/10.1016/j.chempr.2022.07.007

We successfully synthesized a z series of the $A\beta_{17-20}$ peptide (ZLVFF, LZVFF, LVZFF, and LVFZF; Figures 3B and 3C), and we identified that ZLVFF should be the best candidate to inhibit Aβ aggregation. This is because ZLVFF should have strong binding with $A\beta_{13-20}$, whereby the trianionic Z residue can interact with $A\beta_{13-16}$ (HHQK) through electrostatic interactions and hydrogen bonds. The non-protonated histidine residues (N–H on the imidazole rings as hydrogen donors) can form hydrogen bonds with Z residue (hydrogen acceptors), whereas the protonated lysine residue can bind with trianionic Z residue through electrostatic interactions. Here, the LVFF sequence will maintain identical hydrophobic interactions and π-π packing sequences. Thus, the whole segment of HHQKLVFF on the $A\beta_{1-40}$ was designed as the binding site for the POM peptides (e.g., ZLVFF). As shown in Figure 3A, such association is based upon cooperative binding of electrostatic interactions and hydrogen bonding between HHQK ($A\beta_{13-16}$) and POM, as well as hydrophobic interactions and π-π stacking between two LVFF sequences. As LVFF ($A\beta_{17-20}$) is the aggregation core for Aβ peptides,[43] the strong binding between ZLVFF and HHQKLVFF segments on the $A\beta_{1-40}$ can hinder the aggregation of Aβ peptides, therefore preventing them from fibrillation. To interrogate the inhibitory effect of ZLVFF toward Aβ aggregation, a standard thioflavin T (ThT) fluorescence

assay was utilized as ThT can only bind to Aβ aggregates, which increases its fluorescence intensity and thus allows the quantification of Aβ aggregate formation. Incubation of fresh monomeric $A\beta_{1-40}$ alone at 37°C resulted in the characteristic sigmoidal-shaped curve of its ThT fluorescence intensity versus incubation time (Figure 3D).[43] Neither the addition of Z nor of the peptide LVFF had a pronounced effect on Aβ aggregation.

In stark contrast, addition of our POM-AA containing peptide Z-LVFF significantly suppressed the time-dependent increase of ThT fluorescence, indicating its strong inhibitory effect against the formation of amyloid fibrils. LZVFF, LVZFF, and LVFZF all displayed weaker inhibition than ZLVFF as their sequences are not complementary to HHQKLVFF (Figure S27), and 3 negatively charged peptide EEELVFF also showed weaker inhibition than ZLVFF as Z is size-specific toward HHQK (positive electricity cavity-like domain pocket) on $A\beta_{1-40}$, which has been proved recently.[46] To better compare the inhibitory performance of ZLVFF, we evaluated its IC_{50} value using ThT assay (Figures 3E and S28). The IC_{50} value of ZLVFF (10.36 ± 0.72 μM) was approximately 3.8-fold lower than EEELVFF (39.40 ± 2.18 μM), much lower to 90% of high negatively charged POM anions, and comparable to 8 negatively charged Dawson cluster. These results suggested that the inhibition efficiency of ZLVFF was significantly increased due to the multiple interactions between complementary ZLVFF sequence and $A\beta_{1-40}$. Thus, through our facile automated synthesis route, we can readily prepare a family of POM peptides with desirable primary structures, enabling us to investigate and control their biological functions.

Secondary structure control over artificial sequence

After successfully using ZLVFF to disrupt Aβ protein assemblies, we postulated that if we directly inserted Z into a β sheet skeleton, the secondary structure could be modulated because of the high charge density associated with the metal-oxo unit, Z. It is well known that the formation of β sheets is mainly facilitated by multiple backbone hydrogen bonds between different laterally positioned β strands.

Adding the trianionic Z moiety into a peptide sequence should disrupt the original hydrogen bonds between the β strands and should thus transform the β sheet

Please cite this article in press as: She et al., Robotic synthesis of peptides containing metal-oxide-based amino acids, Chem (2022), https://doi.org/10.1016/j.chempr.2022.07.007

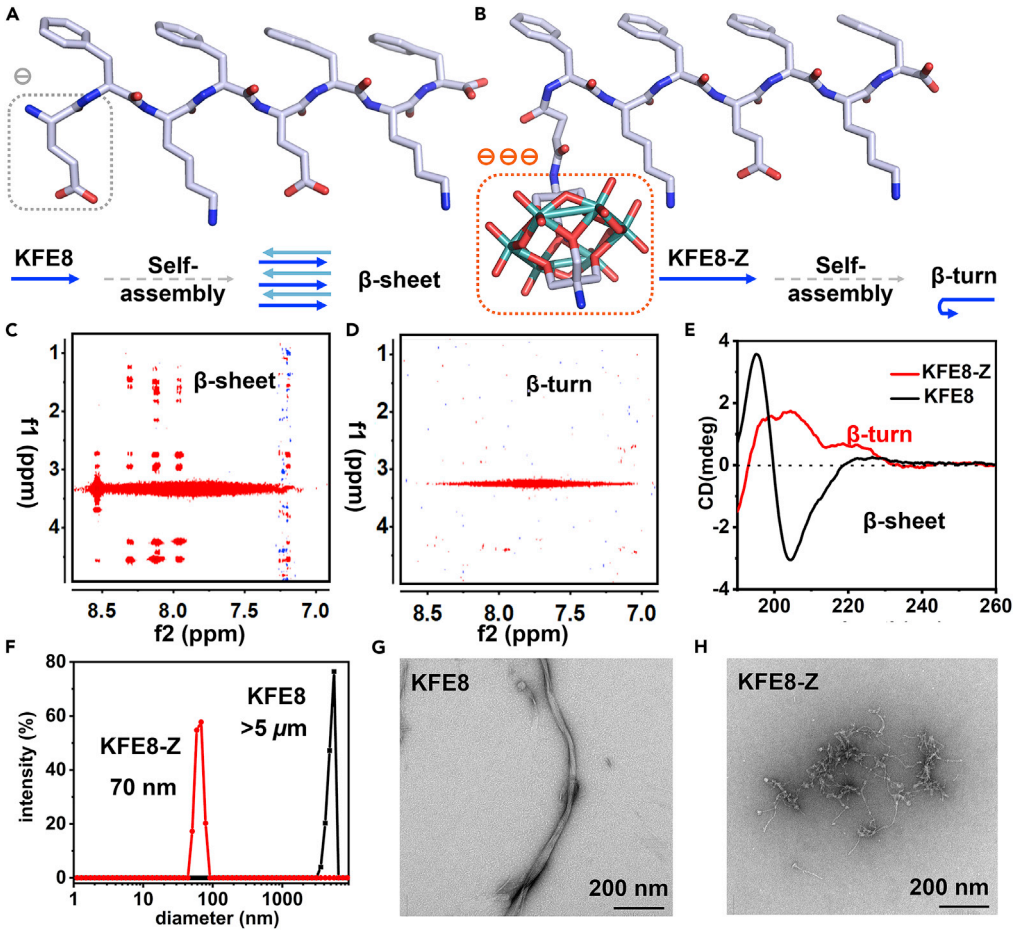

Figure 4. Switching of secondary structure from β sheet to β turn via introducing Z motif

(A) The molecular structure of KFE8; to help understand the self-assembled structures, we use a blue line arrow to represent the peptide chain.

(B) Proposed molecular structure of KFE8-Z drawn by Chimera and Pymol, based on the crystal structure of Z and setting KFE8 as antiparallel β sheet.

(C) NOESY spectra of KFE8; the correlation between the NH (7.98–8.55 ppm) and C$^{\alpha}$H (3.70–4.55 ppm) (Figure S31) , indicating it has strong intermolecular interactions and form an antiparallel β sheet structure that is in accordance with the previously calculated model.

(D) NOESY spectra of KFE8-Z; the disappearance of the correlation between NH (7.98–8.55 ppm) and C$^{\alpha}$H (3.70–4.55 ppm), indicating that it breaks the β sheet structure.

(E) CD spectra of KFE8-Z (red) and KFE8 (black).

(F) DLS spectra of KFE8 and KFE8-Z in H_2O.

(G) TEM images of KFE8 assemblies.

(H) TEM images of KFE8-Z assemblies.

structure into β turn structures, which is another important motif for protein secondary structure and can only be achieve via introducing both proline and glycine motifs. To test this hypothesis, we first selected the artificial peptide sequence KFE8 (EFKFEFKF), which is capable of self-assembling into β sheet because of its amphipathic structure.[48] Then we replaced the singly charged glutamic acid (E) residue at the N terminus of KFE8 with POM-AA (Z) via automated synthesis, Z-FKFEFKF (Figures 4A and 4B). HPLC spectra of KFE8 and KFE8-Z (Figures S7 and S18) demonstrate the high purity of the resultant POM peptide and its parent sequence, which was further confirmed by subsequent ESI-MS measurements (Figures S8 and S19).

To investigate the hydrogen bonding behavior of KFE8 and KFE8-Z, NOESY measurements were conducted. The strong correlation between the NH (7.98–8.55

Please cite this article in press as: She et al., Robotic synthesis of peptides containing metal-oxide-based amino acids, Chem (2022), https://doi.org/10.1016/j.chempr.2022.07.007

ppm) and $C^{\alpha}H$ (3.70–4.55 ppm) (Figures 4C and S31) indicates that there is strong hydrogen bonding between peptide backbones, which is expected for antiparallel β sheet structures.[49] KFE8-Z had no detectable correlation at that range (Figure 4D), indicating that the β sheet structures had been destroyed. We further validated our assumption by performing circular dichroism (CD) spectroscopy to investigate their secondary structures. The CD spectrum of KFE8 (black) exhibited a maximum at 195 nm and a minimum at 204 nm (Figure 4E), suggesting the classical β sheet conformation. Interestingly, the CD spectrum of KFE8-Z (red) revealed several new positive signals of which the most pronounced were at around 200 and 225 nm, which implied a β turn structure.[50]

To investigate self-assembling behaviors of the above peptides, we performed dynamic light scattering (DLS) of aqueous solutions of KFE8-Z and KFE8. The hydrodynamic radius of the supramolecular assembly formed by KFE8 was more than 5 μm (Figure 4F, black), whereas the one from KFE8-Z was only ~70 nm (red). TEM images further supported the above change (Figures 4G and 4H): KFE8 tended to form nanofibers with micron-scale lengths, whereas KFE8-Z simply assembled into nanoaggregates. Such transformation of the secondary structure from β sheet (KFE8) to β turn (KFE8-Z) is likely on account of preferential intramolecular bindings between the oxygen-rich, anionic Z residue and the positively charged lysine residue through electrostatic interaction and hydrogen bonds, as explicated in Figures 4B and S32. Overall, the efficient control over the secondary structure of the artificial peptide sequence was demonstrated through the introduction of POM-AA using automated synthesis.

POM-AA incorporation enhances peptide affinity to the bacterial chaperone DnaK

Next, we wanted to demonstrate that POM peptides were able to engage with a desired biological target, such as a protein, by enhancing hydrogen bonding interactions and thus opening a new avenue toward libraries of potential biological response modifiers. To demonstrate this, the *Escherichia coli* chaperone DnaK was chosen as our model protein. The DnaK/Hsp70 proteins comprise a large, ubiquitous family of ATP-dependent molecular chaperones that converts ATP to ADP during ligand processing. We selected the known DnaK-binding peptide ELPLVKI.[47] The protein structure (Figure 5A) shows that the glutamic acid on this peptide ligand is a major binding contributor and forms multiple hydrogen bonds with $DnaK_{432–436}$ (QSAVT). Considering that POM-AA (Z) is a multivalent hydrogen bond donor, the full oxygen exterior (Figure 5A) may dramatically enhance the binding interactions toward DnaK. Thus, we generated the Z-analog of this peptide using automated peptide synthesis by replacing the N-terminal glutamic acid residue (E) with Z to yield ZLPLVKI.

After expressing and purifying DnaK, we performed microscale thermophoresis (MST) experiments to determine the affinities of both peptides to DnaK (Figure 5B). The affinity of the native peptide sequence (ELPLVKI) was comparable to literature values.[47] Intriguingly, the incorporation of POM-AA led to a 2.5-fold increase in affinity, from 6.4 ± 0.6 μM (ELPLVKI)[51] to 2.8 ± 0.6 μM (ZLPLVKI). We found that POM-AA itself can also bind to DnaK (Figure S34), but the binding is much weaker (K_d = 15.4 ± 0.3 μM) compared with the POM peptide ZLPLVKI. Moreover, we also tried another peptide sequence ELLLRN and ZLLLRN (Figures 5C and S35); the incorporation of POM-AA can endow peptide ligands with the binding affinity toward DnaK protein. Overall, through utilizing the hydrogen bonding donor property of POM-AAs, we can efficiently increase or confer the binding

Please cite this article in press as: She et al., Robotic synthesis of peptides containing metal-oxide-based amino acids, Chem (2022), https://doi.org/10.1016/j.chempr.2022.07.007

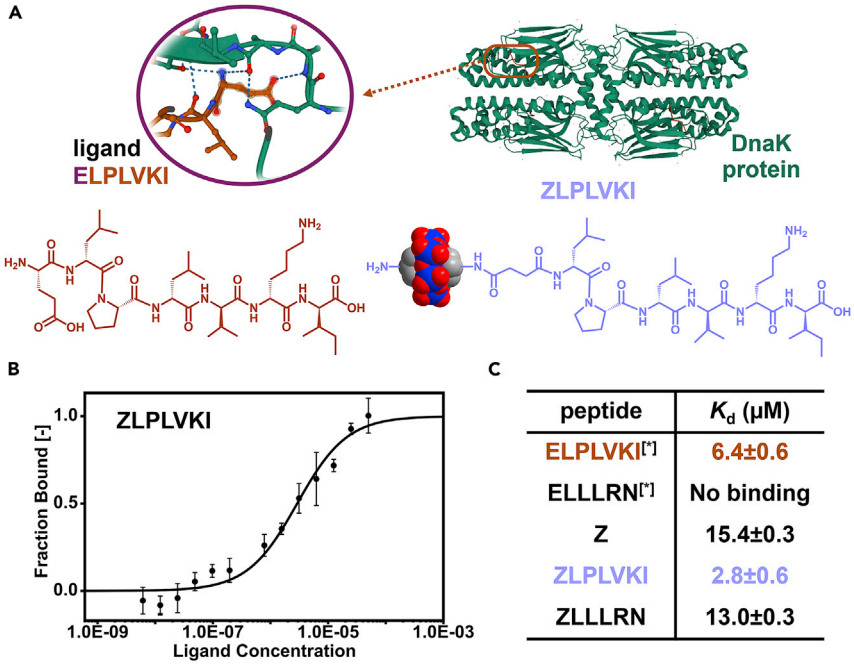

peptide	K_d (μM)
ELPLVKI[*]	6.4±0.6
ELLLRN[*]	No binding
Z	15.4±0.3
ZLPLVKI	2.8±0.6
ZLLLRN	13.0±0.3

Figure 5. Ligand-protein interactions measured with MST

(A) Binding mode of DnaK and ELPLVKI ligand (left); schematic design of ELPLVKI and ZLPLVKI (right).

(B) The binding of ZLPLVKI to DnaK protein is quantified using MST (black dot). The data yield a dissociation constant K_d = 2.8 ± 0.6 μM. The experiments were conducted three times.

(C) The summary table of dissociation constant of 5 peptide ligands toward DnaK protein measured by MST. [*] These dissociation constants are from literature.[47]

affinity to peptide ligand through the introduction of POM-AA using automated synthesis.

Conclusions

We have demonstrated that it is possible to incorporate inorganic amino acids into peptide sequences using automated synthesis on a commercially available peptide synthesizer. The automation, combined with the new building block, allowed the digital control of the sequence that enabled us to explore the great potential of POM peptides, including an entirely new toolbox of configurable architectures as demonstrated here with the amyloid Aβ_{17-20}, amphiphilic KFE8, and bacterial chaperone DnaK substrate. This showed that by combining the peptide backbone with the metal-oxide cluster side chain, it is possible to modulate the structures, including the ability to significantly inhibit amyloid aggregation, switch a β sheet to a β turn, and enhance binding with DnaK protein.

EXPERIMENTAL PROCEDURES

Resource availability

Lead contact

Further information and requests for resources should be directed to and will be fulfilled by the lead contact, Leroy Cronin (lee.cronin@glasgow.ac.uk).

Materials availability

This study did not generate unique reagents.

Please cite this article in press as: She et al., Robotic synthesis of peptides containing metal-oxide-based amino acids, Chem (2022), https://doi.org/10.1016/j.chempr.2022.07.007

Data and code availability

All data supporting the findings of this study are included within the article and its supplemental information and are also available from the authors upon request. Crystallographic data for the structure reported in this paper have been deposited at the Cambridge Crystallographic Data Centre, under the deposition number 2118375. Copies of these data can be obtained free of charge via www.ccdc.cam.ac.uk/structures.

Preparation of POM amino acid

Synthesis of POM-AA

TBA salt of Tris-based Mn-Anderson (38 g, 20 mmol) was dissolved in DMF (400 mL) at 0°C. Succinic anhydride (2.2 g, 22 mmol) was dissolved in DMF (400 mL) and then added dropwise into the above POM solution under stirring. The obtained orange mixture was kept at 25°C for 7 days. After the reaction, the mixture was concentrated to 20 mL through rotary evaporation and precipitated by adding 200 mL diethyl ether (Et_2O) followed with filtration. The resultant orange powder was washed with Et_2O (3 × 100 mL) and then air-dried. This crude product was further purified through crystallization in DMF by Et_2O diffusion. After 1 week, the pure TBA salt of POM-AA were obtained as orange crystals.

Analysis of POM-AA

Yield: 35.4 g, 18.6 mmol, 92 % (based on Mo). Single crystals of POM-AA for X-ray diffraction were grown from DMF and H_2O (one drop) mixture by slow Et_2O diffusion for about 1 month. ^1H NMR (DMSO-d_6, 600 MHz): δ = 0.94 (m, 36H, CH_3), 1.31 (m, 24H, CH_2), 1.57 (m, 24H, CH_2), 2.39 (m, 2H, CH_2), 2.73 (m, 2H, CH_2), 3.17 (m, 24H, CH_2), 12.09 (br, 1H, acid), 62.7 (br, 6H, CH_2), 66.0 (br, 6H, CH_2). Elemental analysis: calc. for $MnMo_6O_{27}C_{60}H_{128}N_5$ (1,982.3 g mol^{-1}): C 36.3 H 6.45 N 3.52; found C 36.3 H 6.46 N 3.53. IR (KBr pellet, 4,000–500 cm^{-1}): 3,289, 2,960, 2,933, 2,873, 1,663, 1,480, 1,382, 1,254, 1,157, 1,100, 1,033, 941, 918, 903, 736, 652, 562 cm^{-1}. The typical peak at 1,030 cm^{-1} can be assigned to Tris-modified Anderson structure. UV-vis (nm): 214, 334.

Counter cation exchange

To ensure its solubility in DMF (the common solvent in peptide synthesis), the POM-AA precursor must contain at least one TBA. Two similar precursors were employed to prepare POM peptides: one uses POM-AA with three TBA counter cations, and the other uses POM-AA with two sodium and one TBA to fulfill certain requirements in applications. To prepare the latter one, the solution of POM-AA with three TBA (1.0 equiv, 0.25 M, CH_3CN) was added dropwise into the solution of sodium perchlorate (50 equiv, 3.125 M, CH_3CN) followed with stirring at 25°C for 1 h. After counter cation exchange, the precipitates were collected by centrifugation and washed with CH_3CN for 3 times. The solid product of POM-AA with two sodium and one TBA salt was dried under vacuum for overnight.

Robotic synthesis of POM peptides

All the POM peptides were prepared through SPPS on a Biotage Initiator + Alstra automated microwave peptide synthesizer.

Synthesis of LZVFF

The POM peptide LZVFF is used here as demonstration. TentaGel S Trt-Phe-Fmoc resin (0.20 mmol/g) was used on 0.1 mmol scale within a 30 mL reactor vial. Fmoc deprotections were performed within piperidine/DMF (20/80, v/v) at 25°C for 3 min, and then repeated for another 10 min. Standard couplings were implemented

at 4 equiv of Fmoc-protected amino acid in DMF, 4.4 equiv of DIC in DMF and 4.4 equiv of HOBt in NMP. A coupling time of 10 min at 75°C was employed for Phe and Val. A coupling time of 60 min at 75°C was employed for POM-AA (three TBA counterions). For Leu (the amino acid right after POM-AA), 10 equiv DIPEA in 4 mL DMF was introduced to wash the resin for 5 min. The subsequent coupling was performed with 4 equiv of $(Fmoc\text{-}Leu)_2O$ anhydride in DMF and 2.5 equiv DIPEA at 75°C for 30 min, and double couplings may further improve the overall yield. After the robotic synthesis, the resin was washed with DCM (3 × 15 mL) and thoroughly dried out. The obtained POM peptides were cleaved from the resin with 10 mL of HFIP:DCM (20:80, v/v) cocktail for 30 min. The crude product with three TBA counter cations was collected through rotary evaporation and washed by 10 mL of cold Et_2O to become orange solid powder.

Synthesis of KFE8-Z

Fmoc-Lys(Mmt)-OH, Fmoc-Glu(OAll), and POM-AA (two sodium and one TBA) were used for the preparation of KEF8-Z, in which the synthetic procedure is same as LZVFF. After on-resin coupling, the subsequent deprotections were performed to remove OAll and/or Mmt before cleavage.[52] For OAll deprotection, 3 equiv $Pd(Ph_3P)_4$ (0.3 mmol, 346.67 mg), 6.66 mL $CHCl_3$, 360 μL acetic acid and 180 μL NMM were used and reacted with the resin at 25°C for 30 min followed by DCM washing (3 × 4 mL). After that, sodium *N*,*N*-diethyldithiocarbamate (0.02 M in DMF, 3 × 4 mL, 15 min) were added to remove Pd. The resin was further washed with DMF (3 × 4 mL) and DCM (3 × 4 mL). For Mmt deprotection, a cleavage cocktail of DCM:TFE:AcOH (70:20:10, v/v/v) were prepared and reacted with the resin at 25°C for 15 min followed by DCM washing (3 × 4 mL). The crude product with three sodium counter cations was cleaved and collected with the same procedure as the above.

Purification of POM peptides

The crude POM peptides were purified through reverse-phase high-performance liquid chromatography (RP-HPLC) on a Phenomenex C18 Kinetic-Evo column with a 5 μm pore size, a 110 Å particle size and with the dimensions 150 × 21.2 mm. A gradient from 5% acetonitrile 95% water to 100% acetonitrile was run with a flow rate of 12 mL/min. Dry peptides were obtained (as TBA salt) by lyophilization and then verified by analytical LC-MS. Analysis of POM peptides was performed by analytical LC-MS on a Bruker MaXis Impact instrument with an Agilent Poroshell 120 EC-C18 (4.6 × 150 mm, 2.7 μm) column. A gradient from 0.1% FA water to 0.1% FA acetonitrile was run with a flow rate of 1 mL/min (Figure S36). The mass peaks and LC traces were analyzed with Compass software. The above methods of purification and analysis have been applied to all the POM peptides.

Analysis of ZLVFF

Yield: 64 mg, 0.026 mmol, 26%. ^1H NMR (DMSO-d_6, 600 MHz): δ = 0.80 (m, 12H, CH_3), 0.94 (m, 36H, CH_3), 1.23–1.81 (m, 32H, CH and CH_2), 2.38 (m, 2H, CH_2), 2.61 (m, 2H, CH_2), 2.74–3.05 (m, 4H, CH), 3.16 (m, 24H, CH_2), 3.51–4.60 (s, 4H, CH_2),7.20 (m, 10H, CH), 7.62 (s, 1H, NH), 8.02 (m, 1H, NH_2), 62.3 (br, 12H, CH_2). Elemental analysis: calc. for $MnMo_6O_{31}C_{89}H_{166}N_9$ (2,489.0 g mol^{-1}): C 43.0 H 6.69 N 5.08; found C 41.3 H 6.77 N 5.00. IR (KBr pellet, 4,000–500 cm^{-1}): 3,291, 2,961, 2,873, 1,637, 1,537, 1,175, 1,100, 1,030, 941, 918, 654, 562 cm^{-1}. The typical peak at 1,030 cm^{-1} can be assigned to Tris-modified Anderson structure. UV-vis (nm): 205, 250, 334.

Sample preparation of POM peptides

All the POM peptides (both TBA and sodium salts) can be readily dissolved in two commonly used solvent systems in peptide research: DMSO and CH_3CN/H_2O

Please cite this article in press as: She et al., Robotic synthesis of peptides containing metal-oxide-based amino acids, Chem (2022), https://doi.org/10.1016/j.chempr.2022.07.007

(50:50, v/v). For subsequent experiments with $A\beta_{1-40}$ and Dnak proteins, the original DMSO solution of POM peptides were further diluted by certain buffers (i.e., HEPES, PBS), to ensure that the volume percentage of DMSO is lower than 5%. In these original and diluted solutions, POM peptides maintain well-dissolved in the solution phase without forming any precipitate.

Pre-treatment of Aβ1–40 sample

Aβ1–40 was purchased from Abcam (ab120479). The powder of Aβ1–40 protein was dissolved in HFIP at the concentration of 1 mg/mL. The resultant solution was shaken at 4°C for 2 h in a sealed vial for complete dissolution. After that, the HFIP was readily removed by evaporation under a gentle stream of N_2. Next, the above operation cycle of dissolution and solvent-removing was repeated twice to guarantee the complete disaggregation of Aβ1–40. The obtained solid sample of Aβ1–40 was further dissolved in 10 mM HEPES buffer (pH 7.4) with 150 mM NaCl.

ThT fluorescence spectroscopy

The kinetics of Aβ aggregations were monitored by using the dye ThT, the fluorescence of which is dependent on the formation of amyloid fibrils. Fluorescence measurements were caried out with a Tecan Infinite 200 PRO plate reader. The fluorescence signal (excitation at 444 nm) was recorded between 460 and 650 nm; 10 nm slites were used for both emission and excitation measurements. The concentrations of Aβ1–40, POM peptides, and ThT were set at 40, 20 and 10 μM, respectively. The fluorescent intensity of aliquots of the Aβ solutions was taken at different time. The original solution of POM peptides were prepared in DMSO and further diluted (20×) by HEPES buffers for subsequent experiments. HEPES buffer contains large amount of sodium, way more than TBA counter cations in the system. Therefore, all the POM peptides can be solely regarded as pure sodium salts, and the effect of highly diluted and ionized TBA counter cations on the aggregation of $A\beta_{1-40}$ peptides can be omitted.

DnaK cloning, culture and purification

The substrate binding domain of DnaK (389–607) was cloned from *Escherichia coli* BL21(DE3) using the following primers: GGATCCgtactgctgctggacgtta and GCAAGCTTGtcaggcatgttgctgctggg. The gene was amplified by PCR with a standard Phusion polymerase protocol with adjusted annealing temperatures then digested by BamHI and HindIII restriction enzymes. The products were subsequently inserted into a pHisTEV plasmids, which was transformed into DH5α(DH3) and Lemo(DE3) strains. A single colony was picked up and expended overnight in Luria-Bertani liquid medium, supplemented with the 50μg/ml of kanamycin. The next day, 1/100 of the cultures were inoculated into fresh Luria-Bertani liquid medium and grown at 37°C and 200 rpm until the OD_{600} reached 0.6–0.8. The cells were thereafter induced with 0.5 mM IPTG for 16 h at 25°C and 200 rpm. Cells were harvested by centrifugation for 15 min at 16°C and 4,000 rpm and the supernatant was discarded. The pellet was weighted and frozen at −80°C until further use.

The bacterial paste was resuspended in the lysis buffer (150 mM NaCl, 20 mM Bis-Tris, pH 6.8 and 1.5 mM β-mercaptoethanol), supplemented with 2 complete EDTA-free protease inhibitor tablets (Sigma-Aldrich) and 4 mg/g DNase (Sigma-Aldrich). Cells were thereafter lysed with the cell disruptor from Microfluidics Corporation at 30 kpi. The lysate was cleared by centrifugation (19,000 rpm, 15 min and 4°C). The supernatant was more thoroughly clarified of the remaining cells debris by filtering through a 0.45 μm filter and applied onto a 5 mL His-Trap FF column (GE Healthcare), pre-equilibrated with the lysis buffer, at a flow rate of 5 mL/min. Bound

proteins were first washed with 10 column volume (CV) of lysis buffer then eluted with 250 μM of imidazole. Factions, containing the protein of interest, were pulled together, and applied into a desalting column (16/10 GE Healthcare, 10 mL/min), pre-equilibrated with the lysis buffer, to remove any presence of imidazole. The His6-tag was also removed by incubating the protein of interests with tobacco etch virus (TEV) protease overnight at 4°C. The His6-tag and uncut proteins were eliminated with a second 5 mL His-Trap FF column run. The flowthroughs were collected and concentrated before injection onto a Superdex 200 16/600 size exclusion column (GE Healthcare), pre-equilibrated in lysis buffer, at a flow rate of 1 mL/min. A final step of concentration to the desired concentration was performed before flash freezing the protein using liquid N_2 and stored at −80°C. The protein concentration was controlled and assessed using photometric analysis (Nanodrop 2000, Thermo Scientific) and the purity was analyzed by SDS-PAGE.

Microscale thermophoresis

MST binding affinity measurements were performed using a Monolith NT 115 system (Nanotemper Technologies). Labeling of different proteins was performed using the Monolith Labeling Kit RED-NHS 2nd generation according to the manufacturer's instructions. For this, a 10 μM dilution of the desired protein was prepared in the supplied labeling buffer NHS (130 mM $NaHCO_3$, 50 mM NaCl, pH 8.2). To yield a 600 μM dye solution, 25 μL DMSO was added to dry powder. For the labeling procedure, 7 μL of the freshly prepared dye solution was mixed with 7 μL of the labeling buffer NHS. Subsequently, 10 μL of the diluted dye solution were added to 90 μL of the diluted protein to yield a 3-fold molar excess of dye. The mixture was kept in the dark for 30 min at room temperature. Subsequently, the labeled protein was separated from excess dye using the supplied B-column equilibrated in gel filtration buffer + 0.05% Tween-20. The final concentration of the labeled protein was determined via UV-vis spectrometry. Afterwards, the labeled protein was either used immediately for MST measurements or stored for further use by flash freezing in liquid N_2.

In preparation for a MST measurement, a buffer exchange of the desired ligand into the same buffer was performed. Serial ligand dilutions were created according to the manufacturer's instructions, with the maximum ligand concentration adjusted to the expected K_d. The MST experiment was carried out at 25°C with an automatically detected excitation power, the MST power was set to medium. The subsequent measurements required to achieve biological triplicates were performed with the previously determined excitation power. A K_d measurement with standard error was calculated using the MO. Affinity Analysis v2.3 software.

SUPPLEMENTAL INFORMATION

Supplemental Information can be found online at https://doi.org/10.1016/j.chempr.2022.07.007.

ACKNOWLEDGMENTS

This work was supported by the EPSRC grants (no. EP/J015156/1; EP/L023652/1; EP/I033459/1; EP/ J015156/1; EP/K023004/1; and EP/L023652/1), the European Research Council (project 670467 SMART-POM), and the University of Glasgow. S.S. acknowledges Marie Skłodowska-Curie Fellowship (PPOM-PTT, 798821) J.K. acknowledges the funding by European Research Council (ERC Consolidator Grant 101002326).

AUTHOR CONTRIBUTIONS

L.C. came up with the concept, and S.S. and L.C. developed the idea and the synthetic approach. S.S., N.L.B, J.S.M, M.D.C., D.-L.L., and J.K. designed the experiments. S.S. executed most of the experiments and analyzed the data. D.Z. conducted the DnaK protein preparation and following MST test. J.S.M., M.D.C., and D.-L.L. helped perform mass spectra, single-crystal X-ray diffraction, and data analysis. S.S., N.L.B, D.-L.L., J.K., and L.C. wrote the manuscript. All authors discussed the experiments, edited the manuscript, and gave consent for this publication under the supervision of L.C.

DECLARATION OF INTERESTS

The authors declare no competing interests.

Received: March 21, 2022
Revised: May 11, 2022
Accepted: July 8, 2022
Published: August 8, 2022

REFERENCES

1. Mehr, S.H.M., Craven, M., Leonov, A.I., Keenan, G., and Cronin, L. (2020). A universal system for digitization and automatic execution of the chemical synthesis literature. Science *370*, 101–108. https://doi.org/10.1126/science.abc2986.

2. Steiner, S., Wolf, J., Glatzel, S., Andreou, A., Granda, J.M., Keenan, G., Hinkley, T., Aragon-Camarasa, G., Kitson, P.J., Angelone, D., and Cronin, L. (2019). Organic synthesis in a modular robotic system driven by a chemical programming language. Science *363*, 122–130. https://doi.org/10.1126/science.aav2211.

3. Merrifield, R.B. (1965). Automated synthesis of peptides. Science *150*, 178–185. https://doi.org/10.1126/science.150.3693.178.

4. Plante, O.J., Palmacci, E.R., and Seeberger, P.H. (2001). Automated solid-phase synthesis of oligosaccharides. Science *291*, 1523–1527. https://doi.org/10.1126/science.1057324.

5. Alvarado-Urbina, G., Sathe, G.M., Liu, W.C., Gillen, M.F., Duck, P.D., Bender, R., and Ogilvie, K.K. (1981). Automated synthesis of gene fragments. Science *214*, 270–274. https://doi.org/10.1126/science.6169150.

6. Li, J., Ballmer, S.G., Gillis, E.P., Fujii, S., Schmidt, M.J., Palazzolo, A.M.E., Lehmann, J.W., Morehouse, G.F., and Burke, M.D. (2015). Synthesis of many different types of organic small molecules using one automated process. Science *347*, 1221–1226. https://doi.org/10.1126/science.aaa5414.

7. Liu, C., Xie, J., Wu, W., Wang, M., Chen, W., Idres, S.B., Rong, J., Deng, L.-W., Khan, S.A., and Wu, J. (2021). Automated synthesis of prexasertib and derivatives enabled by continuous-flow solid-phase synthesis. Nat. Chem. *13*, 451–457. https://doi.org/10.1038/s41557-021-00662-w.

8. Angelone, D., Hammer, A.J.S., Rohrbach, S., Krambeck, S., Granda, J.M., Wolf, J., Zalesskiy, S., Chisholm, G., and Cronin, L. (2021). Convergence of multiple synthetic paradigms in a universally programmable chemical synthesis machine. Nat. Chem. *13*, 63–69. https://doi.org/10.1038/s41557-020-00596-9.

9. Burger, B., Maffettone, P.M., Gusev, V.V., Aitchison, C.M., Bai, Y., Wang, X., Li, X., Alston, B.M., Li, B., Clowes, R., et al. (2020). A mobile robotic chemist. Nature *583*, 237–241. https://doi.org/10.1038/s41586-020-2442-2.

10. Garcia, A.M., Iglesias, D., Parisi, E., Styan, K.E., Waddington, L.J., Deganutti, C., De Zorzi, R., Grassi, M., Melchionna, M., Vargiu, A.V., and Marchesan, S. (2018). Chirality effects on peptide self-assembly unraveled from molecules to materials. Chem *4*, 1862–1876. https://doi.org/10.1016/j.chempr.2018.05.016.

11. Abbas, M., Lipiński, W.P., Nakashima, K.K., Huck, W.T.S., and Spruijt, E. (2021). A short peptide synthon for liquid–liquid phase separation. Nat. Chem. *13*, 1046–1054. https://doi.org/10.1038/s41557-021-00788-x.

12. Wu, D., Sinha, N., Lee, J., Sutherland, B.P., Halaszynski, N.I., Tian, Y., Caplan, J., Zhang, H.V., Saven, J.G., Kloxin, C.J., and Pochan, D.J. (2019). Polymers with controlled assembly and rigidity made with click-functional peptide bundles. Nature *574*, 658–662. https://doi.org/10.1038/s41586-019-1683-4.

13. Ng, C.C.A., Tam, W.M., Yin, H., Wu, Q., So, P.-K., Wong, M.Y.-M., Lau, F.C.M., and Yao, Z.-P. (2021). Data storage using peptide sequences. Nat. Commun. *12*, 4242. https://doi.org/10.1038/s41467-021-24496-9.

14. Sawada, T., and Fujita, M. (2020). Folding and assembly of metal-linked peptidic nanostructures. Chem *6*, 1861–1876. https://doi.org/10.1016/j.chempr.2020.07.002.

15. Liu, Q., Wan, K., Shang, Y., Wang, Z.-G., Zhang, Y., Dai, L., Wang, C., Wang, H., Shi, X., Liu, D., and Ding, B. (2021). Cofactor-free oxidase-mimetic nanomaterials from self-assembled histidine-rich peptides. Nat. Mater. *20*, 395–402. https://doi.org/10.1038/s41563-020-00856-6.

16. Tsvirkun, D., Ben-Nun, Y., Merquiol, E., Zlotver, I., Meir, K., Weiss-Sadan, T., Matok, I., Popovtzer, R., and Blum, G. (2018). CT imaging of enzymatic activity in cancer using covalent probes reveal a size-dependent pattern. J. Am. Chem. Soc. *140*, 12010–12020. https://doi.org/10.1021/jacs.8b05817.

17. Su, D., Gao, L., Gao, F., Zhang, X., and Gao, X. (2020). Peptide and protein modified metal clusters for cancer diagnostics. Chem. Sci. *11*, 5614–5629. https://doi.org/10.1039/D0SC01201G.

18. Connah, L., and Angelovski, G. (2020). Solid phase synthesis in the development of magnetic resonance imaging probes. Org. Chem. Front. *7*, 4121–4141. https://doi.org/10.1039/D0QO00921K.

19. Wang, M., Song, Y., Zhang, S., Zhang, X., Cai, X., Lin, Y., De Yoreo, J.J., and Chen, C.-L. (2021). Programmable two-dimensional nanocrystals assembled from POSS-containing peptoids as efficient artificial light-harvesting systems. Sci. Adv. *7*, eabg1448. https://doi.org/10.1126/sciadv.abg1448.

20. Kreidt, E., Leis, W., and Seitz, M. (2020). Direct solid-phase synthesis of molecular heterooligonuclear lanthanoid-complexes. Nat. Commun. *11*, 1346. https://doi.org/10.1038/s41467-020-15199-8.

21. van Staveren, D.R., and Metzler-Nolte, N. (2004). Bioorganometallic chemistry of ferrocene. Chem. Rev. *104*, 5931–5985. https://doi.org/10.1021/cr0101510.

22. Luo, D., Wang, X., Walker, E., Wang, J., Springer, S., Lou, J., Ramamurthy, G., Burda, C., and Basilion, J.P. (2020). Nanoparticles yield increased drug uptake and therapeutic efficacy upon sequential near-infrared irradiation. ACS Nano *14*, 15193–15203. https://doi.org/10.1021/acsnano.0c05425.

23. Mirts, E.N., Bhagi-Damodaran, A., and Lu, Y. (2019). Understanding and modulating metalloenzymes with unnatural amino acids,

non-native metal ions, and non-native metallocofactors. Acc. Chem. Res. *52*, 935–944. https://doi.org/10.1021/acs.accounts.9b00011.

24. Pyles, H., Zhang, S., De Yoreo, J.J., and Baker, D. (2019). Controlling protein assembly on inorganic crystals through designed protein interfaces. Nature *571*, 251–256. https://doi.org/10.1038/s41586-019-1361-6.

25. Addadi, L., Joester, D., Nudelman, F., and Weiner, S. (2006). Mollusk shell formation: a source of new concepts for understanding biomineralization processes. Chemistry *12*, 980–987. https://doi.org/10.1002/chem.200500980.

26. Harris, F., Dennison, S.R., and Phoenix, D.A. (2013). Anionic antimicrobial peptides. Antimicrob. Pept. 83–113.

27. Hamley, I.W. (2012). The amyloid beta peptide: a chemist's perspective. Role in Alzheimer's and fibrillization. Chem. Rev. *112*, 5147–5192. https://doi.org/10.1021/cr3000994.

28. Yvon, C., Surman, A.J., Hutin, M., Alex, J., Smith, B.O., Long, D.-L., and Cronin, L. (2014). Polyoxometalate clusters integrated into peptide chains and as inorganic amino acids: solution- and solid-phase approaches. Angew. Chem. Int. Ed. Engl. *53*, 3336–3341. https://doi.org/10.1002/anie.201311135.

29. Soria-Carrera, H., Franco-Castillo, I., Romero, P., Martín, S., de la Fuente, J.M., Mitchell, S.G., and Martín-Rapún, R. (2021). On-POM ring-opening polymerisation of N-carboxyanhydrides. Angew. Chem. Int. Ed. Engl. *60*, 3449–3453. https://doi.org/10.1002/anie.202013563.

30. Pope, M.T., and Müller, A. (1991). Polyoxometalate chemistry: an old field with new dimensions in several disciplines. Angew. Chem. Int. Ed. Engl. *30*, 34–48. https://doi.org/10.1002/anie.199100341.

31. Liu, T., Diemann, E., Li, H., Dress, A.W.M., and Müller, A. (2003). Self-assembly in aqueous solution of wheel-shaped Mo154 oxide clusters into vesicles. Nature *426*, 59–62. https://doi.org/10.1038/nature02036.

32. Chen, X., Zhang, G., Li, B., and Wu, L. (2021). An integrated giant polyoxometalate complex for photothermally enhanced catalytic oxidation. Sci. Adv. *7*, eabf8413. https://doi.org/10.1126/sciadv.abf8413.

33. Chen, J.-J., Symes, M.D., and Cronin, L. (2018). Highly reduced and protonated aqueous solutions of $[P_2W_{18}O_{62}]^{6-}$ for on-demand hydrogen generation and energy storage. Nat. Chem. *10*, 1042–1047. https://doi.org/10.1038/s41557-018-0109-5.

34. She, S., Xuan, W., Bell, N.L., Pow, R., Ribo, E.G., Sinclair, Z., Long, D.-L., and Cronin, L. (2020). Peptide sequence mediated self-assembly of molybdenum blue nanowheel superstructures. Chem. Sci. *12*, 2427–2432. https://doi.org/10.1039/D0SC06098D.

35. Rhule, J.T., Hill, C.L., Judd, D.A., and Schinazi, R.F. (1998). Polyoxometalates in medicine. Chem. Rev. *98*, 327–358. https://doi.org/10.1021/cr960396q.

36. Tagliavini, V., Honisch, C., Serratì, S., Azzariti, A., Bonchio, M., Ruzza, P., and Carraro, M. (2021). Enhancing the biological activity of polyoxometalate-peptide nano-fibrils by spacer design. RSC Adv. *11*, 4952–4957. https://doi.org/10.1039/D0RA10218K.

37. Ventura, D., Calderan, A., Honisch, C., Krol, S., Serratì, S., Bonchio, M., Carraro, M., and Ruzza, P. (2018). Synthesis and biological activity of an Anderson polyoxometalate bis-functionalized with a bombesin-analog peptide. Pept. Sci. *110*, e24047. https://doi.org/10.1002/pep2.24047.

38. Salazar Marcano, D.E., Lentink, S., Moussawi, M.A., and Parac-Vogt, T.N. (2021). Solution dynamics of hybrid Anderson-Evans polyoxometalates. Inorg. Chem. *60*, 10215–10226. https://doi.org/10.1021/acs.inorgchem.1c00511.

39. Li, J., Chen, Z., Zhou, M., Jing, J., Li, W., Wang, Y., Wu, L., Wang, L., Wang, Y., and Lee, M. (2016). Polyoxometalate-driven self-assembly of short peptides into multivalent nanofibers with enhanced antibacterial activity. Angew. Chem. Int. Ed. Engl. *55*, 2592–2595. https://doi.org/10.1002/anie.201511276.

40. Guo, H., Zeng, M., Li, X., He, H., Wu, L., and Li, H. (2021). Multifunctional enhancement of proton-conductive, stretchable, and adhesive performance in hybrid polymer electrolytes by polyoxometalate nanoclusters. ACS Appl. Mater. Interfaces *13*, 30039–30050. https://doi.org/10.1021/acsami.1c06848.

41. Anyushin, A.V., Kondinski, A., and Parac-Vogt, T.N. (2020). Hybrid polyoxometalates as post-functionalization platforms: from fundamentals to emerging applications. Chem. Soc. Rev. *49*, 382–432. https://doi.org/10.1039/C8CS00854J.

42. Hasenknopf, B., Delmont, R., Herson, P., and Gouzerh, P. (2002). Anderson-type heteropolymolybdates containing tris(alkoxo) ligands: synthesis and structural characterization. Eur. J. Inorg. Chem. *2002*, 1081–1087. https://doi.org/10.1002/1099-0682(200205)2002:5<1081::AID-EJIC1081>3.0.CO;2-W.

43. Takahashi, T., and Mihara, H. (2008). Peptide and protein mimetics inhibiting amyloid β-peptide aggregation. Acc. Chem. Res. *41*, 1309–1318. https://doi.org/10.1021/ar8000475.

44. Geng, J., Li, M., Ren, J., Wang, E., and Qu, X. (2011). Polyoxometalates as inhibitors of the aggregation of amyloid β peptides associated with Alzheimer's disease. Angew. Chem. Int. Ed. Engl. *50*, 4184–4188. https://doi.org/10.1002/anie.201007067.

45. Gao, N., Sun, H., Dong, K., Ren, J., Duan, T., Xu, C., and Qu, X. (2014). Transition-metal-substituted polyoxometalate derivatives as functional anti-amyloid agents for Alzheimer's disease. Nat. Commun. *5*, 3422. https://doi.org/10.1038/ncomms4422.

46. Gao, N., Du, Z., Guan, Y., Dong, K., Ren, J., and Qu, X. (2019). Chirality-selected chemical modulation of amyloid aggregation. J. Am. Chem. Soc. *141*, 6915–6921. https://doi.org/10.1021/jacs.8b12537.

47. Gao, N., Liu, Z., Zhang, H., Liu, C., Yu, D., Ren, J., and Qu, X. (2022). Site-directed chemical modification of amyloid by polyoxometalates for inhibition of protein misfolding and aggregation. Angew. Chem. Int. Ed. Engl. *61*. e202115336. https://doi.org/10.1002/anie.202115336.

48. Marini, D.M., Hwang, W., Lauffenburger, D.A., Zhang, S., and Kamm, R.D. (2002). Left-handed helical ribbon intermediates in the self-assembly of a β-sheet peptide. Nano Lett. *2*, 295–299. https://doi.org/10.1021/nl015697g.

49. Åslund, F., Nordstrand, K., Berndt, K.D., Nikkola, M., Bergman, T., Ponstingl, H., Jörnvall, H., Otting, G., and Holmgren, A. (1996). Glutaredoxin-3 from *Escherichia coli*: amino acid sequence, 1H and 15N NMR assignments, and structural analysis (*). J. Biol. Chem. *271*, 6736–6745. https://doi.org/10.1074/jbc.271.12.6736.

50. Clarke, D.E., Wu, G., Wu, C., and Scherman, O.A. (2021). Host-guest induced peptide folding with sequence-specific structural chirality. J. Am. Chem. Soc. *143*, 6323–6327. https://doi.org/10.1021/jacs.1c00342.

51. Zahn, M., Berthold, N., Kieslich, B., Knappe, D., Hoffmann, R., and Sträter, N. (2013). Structural studies on the forward and reverse binding modes of peptides to the chaperone DnaK. J. Mol. Biol. *425*, 2463–2479. https://doi.org/10.1016/j.jmb.2013.03.041.

52. Isidro-Llobet, A., Álvarez, M., and Albericio, F. (2009). Amino acid-protecting groups. Chem. Rev. *109*, 2455–2504. https://doi.org/10.1021/cr800323s.